

## ARTICLE OPEN



# Contributions of sea–land breeze and local climate zones to daytime and nighttime heat island intensity

Jun Yang<sup>1,2,✉</sup>, Jiaying Xin<sup>1</sup>, Yuqing Zhang<sup>1,✉</sup>, Xiangming Xiao<sup>3</sup> and Jianhong Cecilia Xia<sup>4</sup>

The acceleration of global urbanization has increased the frequency of the urban heat island (UHI) effect and heatwaves, which seriously endanger human health. We used Shenzhen as a case study to examine the daytime and nighttime differences in UHI intensity (UHII), considering different local climate zones (LCZs) and sea–land breezes. The diurnal UHII was  $>3\text{ }^{\circ}\text{C}$  for 52% of the study period, whereas the nocturnal UHII was  $>3\text{ }^{\circ}\text{C}$  for only 26% of the study period. The average diurnal and nocturnal building-type UHII values were 2.77 and 1.11  $^{\circ}\text{C}$  higher than those of the natural type, respectively. Sea breezes alleviated the UHI effect with a linear correlation coefficient of  $-0.68601$  between them. Moreover, diurnal and nocturnal UHII showed differences across different gradients, which can help guide urban planning.

*npj Urban Sustainability* (2022)2:12; <https://doi.org/10.1038/s42949-022-00055-z>

## INTRODUCTION

Urbanization has been accelerating since the beginning of the 21st century<sup>1–3</sup>. In China, as the population increases annually<sup>4</sup>, the areas under impervious layers have also witnessed increases, causing surface temperatures to increase and exacerbate the urban heat island (UHI) effect, extreme weather, and heat waves<sup>5–8</sup>, all of which affect human comfort and threaten human health<sup>9–13</sup>, and even cause death. The UHI phenomenon was first discovered by Howard<sup>14</sup>, who conducted temperature observations in London, UK, and urban thermal environments have been the subject of active research ever since.

Land surface temperature is an important parameter for urban thermal environment research<sup>15</sup>; therefore, many international studies have investigated methods to determine it. Compared with traditional meteorological station observations, thermal infrared (TIR) image data can retrieve land surface temperature more effectively. Owing to the advantages of this method, such as its spatial continuity and easily accessible images, it has been widely used in research on UHIs<sup>16–22</sup>. Depending on the source of the image sensor, TIR images can include high, medium, and low spatial resolution data, such as Landsat/TIRS (100 m), ASTER (90 m), GF5/VIMS (40 m), HJ-1B/IRS (300 m), and MODIS (1000 m). Presently, studies on urban thermal environments commonly use Landsat TM/TIRS or MODIS data for land surface temperature inversion and UHI intensity (UHII) calculations, resulting in the development of heat island mitigation strategies<sup>18,20,23–31</sup>. However, the former is difficult to acquire at night, whereas the latter has a low resolution and cannot accurately analyze thermal environments at the urban-block scale. Therefore, MODIS data are more suitable for large-scale research on regional thermal environments. ASTER data have a high spatial resolution and can provide suitable night images. These data have become the main source for daytime and nighttime UHI research, respectively; therefore, AST\_08 data were used in this study to conduct land surface temperature inversion calculations.

UHIs are affected by many factors, including architecture, climate, and land map<sup>32–38</sup>. However, owing to rapid urbanization

in China, available morphological and land-use data are inevitably unstandardized, difficult to obtain, or cannot be used for urban planning or environmental research. The local climate zone (LCZ) classification scheme constitutes a climate-related land cover classification system for urban structures, which was first proposed by Stewart et al.<sup>39,40</sup>. This classification scheme has been used worldwide as an international standard for climate-related research<sup>41–43</sup> and is widely used in UHI research<sup>44–49</sup>. Presently, LCZ classification methods can primarily be divided into two types. The first uses the World City Database Portal Tool (WUDAPT)<sup>50–53</sup>; the software required for this method is free, and the data are easily obtainable, but its spatial resolution is low; thus, it is only suitable for large-scale research. The second method uses a geographic information system (GIS) to calculate building parameters and vegetation indicators to divide LCZs into smaller study units<sup>54–57</sup>. Although obtaining data for this method is more difficult, the classification results correspond well with the actual field conditions. Therefore, the second classification method was used herein and building and land-use data were combined to classify the LCZs.

Recent studies have shown that urban ventilation can improve urban thermal comfort and alleviate the UHI effect<sup>58–61</sup>. Sea and land breezes, representative of typical local winds in coastal cities and which alternate during days and nights, refer to the mesoscale circulations formed via the temperature difference between the ocean and land. As they frequently occur in coastal cities, previous research has attempted to address the interactions between sea and land breezes and UHIs<sup>62–65</sup>. For instance, Sangobanwo<sup>66</sup> revealed that coastal cities are more susceptible to UHIs due to sea–land breezes and are generally more prone to extremely high temperatures than inland cities. Wang et al.<sup>67</sup> used the Weather Research and Forecasting (WRF) model to simulate the sea–land breeze and thermal environment, further analyzing its effect on the UHI. Shen and Yuan<sup>68</sup> used the large eddy simulation module in the WRF model to simulate five urban cases and one non-urban case. They analyzed the interactions between sea–land breezes and UHIs, and found that sea–land breeze circulation was stronger in urban areas; moreover, they revealed

<sup>1</sup>Human Settlements Research Center, Liaoning Normal University, 116029 Dalian, China. <sup>2</sup>Jangho Architecture College, Northeastern University, 110169 Shenyang, China.

<sup>3</sup>Department of Microbiology and Plant Biology, Center for Spatial Analysis, University of Oklahoma, Norman, OK 73019, USA. <sup>4</sup>School of Earth and Planetary Sciences (EPS), Curtin University, Perth, WA 65630, Australia. ✉email: yangjun8@mail.neu.edu.cn; zhangyuqing@lnnu.edu.cn

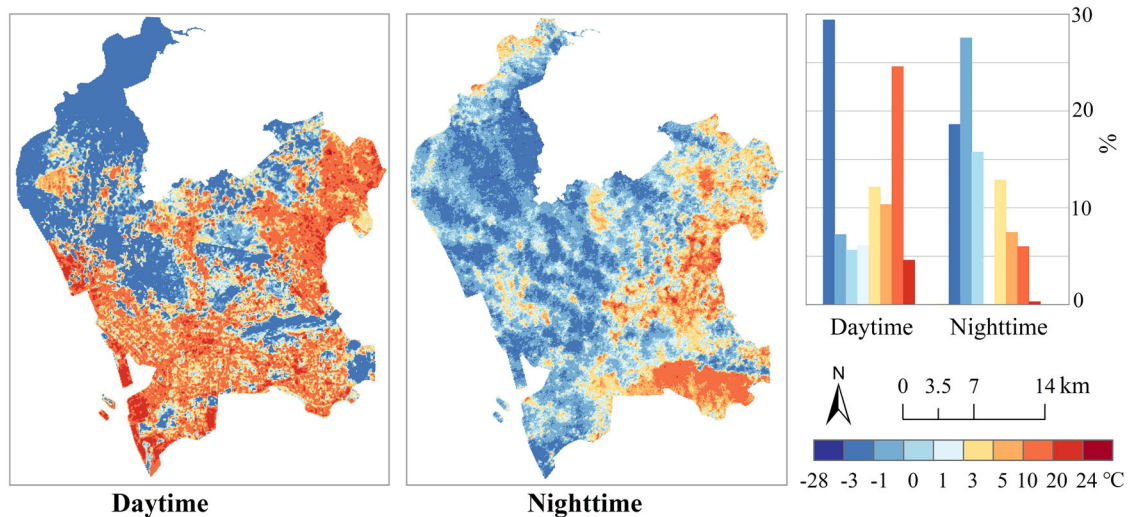


**Fig. 1** Daytime and nighttime heat island spatial distribution map and the percentage of daytime and nighttime UHII in each category. All daytime and nighttime UHII values are shown, and the UHII grading standard is also shown. The bar chart shows the proportion of different grades of UHII.

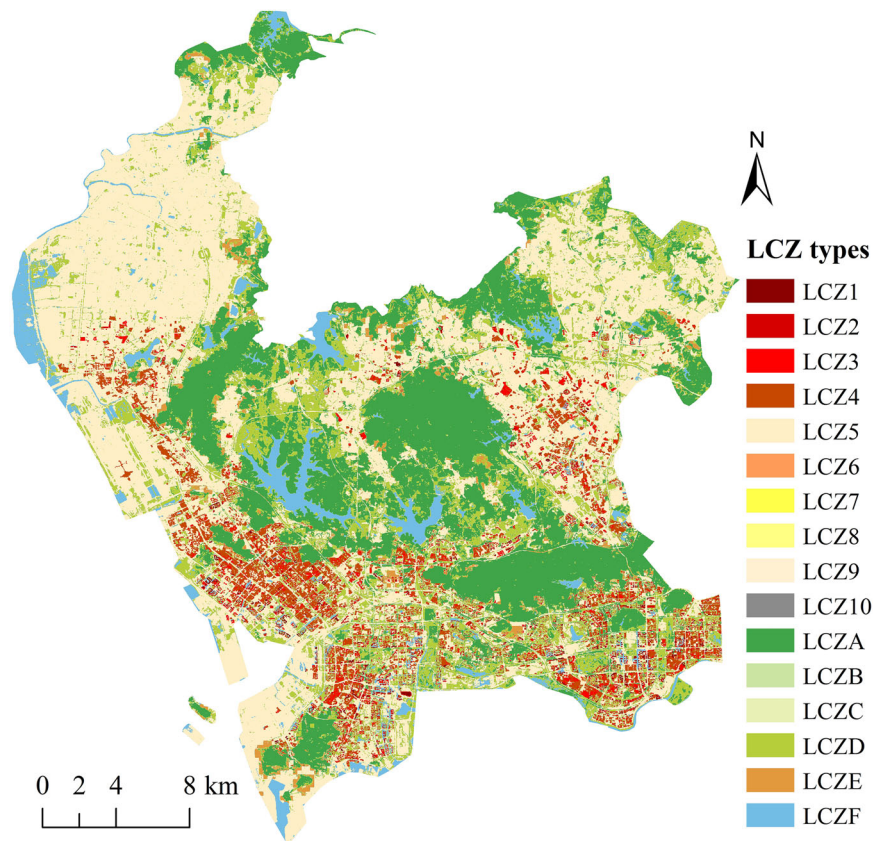


**Fig. 2** LCZ spatial distribution. LCZ1-10 and LCZA-F respectively represent different LCZ types.

that UHIs were alleviated when the wind speed was high and sea breezes flooded city interior. Sea-land breezes can also significantly affect UHIs. However, most studies have only qualitatively analyzed the weakening effect of sea breeze on the strength of the heat island. Few studies analyze the correlation between sea and land wind speed and UHII. In addition, discussing the strength of the sea and land breeze and heat island under different gradients (distance from the coastline) is necessary. This has

important implications for urban planning and a rational layout of the city. Therefore, in this study, the effects of sea-land breezes on the daytime and nighttime UHIs were analyzed under different gradients based on meteorological data.

The main purpose of this study was to explore the internal differences in the urban thermal environment of Shenzhen from the perspective of LCZs and sea-land breezes. The main objectives were to: (1) analyze the UHII day and night spatial

differences based on the land surface temperature directly calculated from AST\_08 images, (2) analyze the influence of different LCZ types on the intensity of heat islands based on Oke's classification standard for LCZs, and (3) analyze the daily variation in the UHIs between typical and atypical sea and land breeze days based on weather station data, and investigate the influence of the sea and land wind speeds on the intensity of heat islands under different gradients using correlation analysis. This study can provide a reference for urban planning and for mitigating the UHI effect.

## RESULTS

### Daytime and nighttime UHI and LCZ spatial distributions

Overall, the daytime and nighttime UHI spatial distributions (Fig. 1) were highly consistent with the spatial distribution of the

LCZ type (Fig. 2). Among these (Table 1), a large amount of building-type data were collected from the eastern Longhua District, and in the southeastern Bao'an, Nanshan, and Futian districts. The order of the LCZs of residential areas was  $LCZ5 > LCZA > LCZD > LCZF > LCZ4 > LCZ10 > LCZ3 > LCZE > LCZB > LCZ1 > LCZ2 > LCZ9 > LCZC > LCZ8 > LCZ6 > LCZ7$ . Moreover, the proportion of natural types in Bao'an, Longhua, Futian, and Nanshan Districts was higher than that of building types (Bao'an District:  $0.240 > 0.233$ , Longhua District:  $0.113 > 0.106$ , Futian District:  $0.064 > 0.027$ , Nanshan District:  $0.156 > 0.062$ ). Among these, Bao'an and Longhua districts collected large-scale data on LCZ5, LCZA, LCZD, LCZE, and LCZF. In particular, the corresponding daytime and nighttime UHI values were relatively high for compact super high-rise (LCZ1), compact high-rise (LCZ2), compact mid-high-rise (LCZ3), and compact mid-rise (LCZ4) buildings. Meanwhile, a large amount of natural type data (LCZA–LCZF) and compact low-rise buildings (LCZ5) were present in western Bao'an District and western Longhua District, but the corresponding daytime and nighttime UHI values were low. Therefore, these building types (LCZ1–LCZ10) corresponded to higher UHI values, whereas the natural types (LCZA–LCZF) corresponded to lower UHI values. In addition, the statistics on the proportions of the daytime and nighttime UHI values revealed that the nighttime UHI values were lower than those during the daytime (Fig. 1). During the day, the UHI was  $>3^\circ\text{C}$  for 52% of the study period, which was only true for 26% of the study period at night. For the negative heat island, the maximum intensity ( $<-3^\circ\text{C}$ ) also showed that day (29%)  $>$  night (19%); however, the

Location	LCZ types	Proportion	Location	LCZ types	Proportion
Bao'an District	LCZ1	0.0005679	Longhua District	LCZ1	0.0000686
	LCZ2	0.0010569		LCZ2	0.0003087
	LCZ3	0.0016498		LCZ3	0.0007032
	LCZ4	0.0106007		LCZ4	0.0027107
	LCZ5	0.2190609		LCZ5	0.1021162
	LCZ10	0.0002152		LCZA	0.0429196
	LCZA	0.0791994		LCZB	0.0000348
	LCZB	0.0001515		LCZD	0.0553085
	LCZD	0.0995902		LCZE	0.0033539
	LCZE	0.0111709		LCZF	0.0109850
Futian District	LCZF	0.0494042	Nanshan District	LCZ1	0.0008761
	LCZ1	0.0009103		LCZ2	0.0007673
	LCZ2	0.0009642	LCZ3	0.0011543	
	LCZ3	0.0015457	LCZ4	0.0070949	
	LCZ4	0.0041295	LCZ5	0.0516130	
	LCZ5	0.0190421	LCZ9	0.0001254	
	LCZ10	0.0000933	LCZ10	0.0003969	
	LCZA	0.0255055	LCZA	0.0597380	
	LCZB	0.0000614	LCZB	0.0004056	
	LCZD	0.0323152	LCZD	0.0666401	
LCZE	0.0012252	LCZE	0.0078832		
LCZF	0.0052551	LCZF	0.0210808		

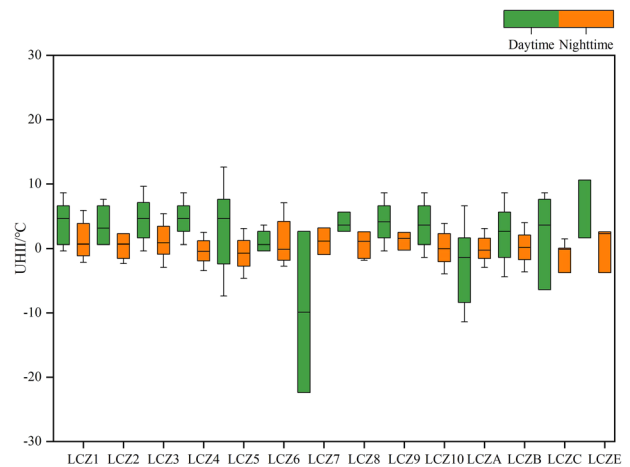


**Fig. 3** The difference of day and night UHI corresponding to each LCZ types. NUHI is the nighttime UHI and DUHI is the daytime UHI.

LCZ types	Nighttime ( $^\circ\text{C}$ )	Daytime ( $^\circ\text{C}$ )	LCZ types	Nighttime ( $^\circ\text{C}$ )	Daytime ( $^\circ\text{C}$ )
LCZ1	1.48	1.95	LCZA	-0.48	-5.31
LCZ2	1.16	1.69	LCZB	0.30	-0.17
LCZ3	0.75	3.01	LCZC	-0.43	-0.31
LCZ4	0.35	3.14	LCZE	-0.80	0.71
LCZ5	-0.84	-0.15			
LCZ6	0.21	1.10			
LCZ7	2.20	0.18			
LCZ8	1.46	1.49			
LCZ9	0.84	2.07			
LCZ10	-0.02	0.48			

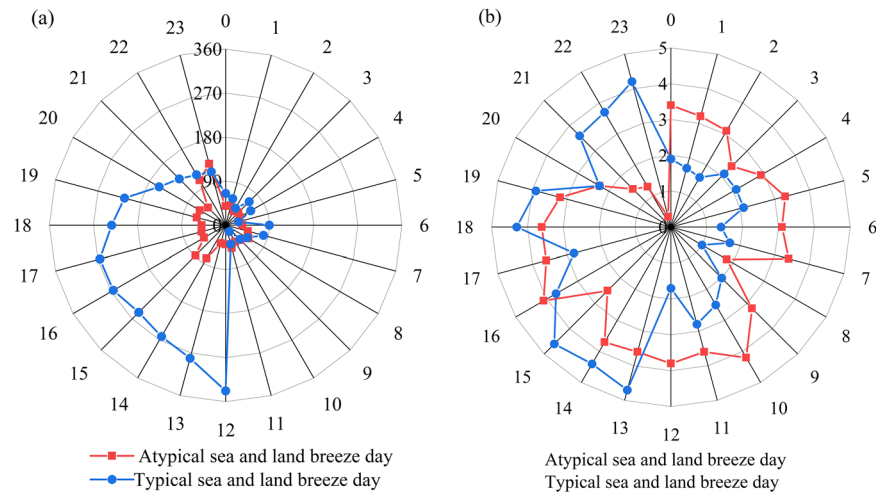


**Fig. 4** Diurnal changes in wind speed and direction between typical sea and land breeze day and atypical sea and land breeze day. **a** Wind direction, **b** wind speed.

UHI values in each interval, ranging from  $-1$  to  $3$  °C, show that the proportion at night is greater than that during the day (28% (night) > 7% (day), 16% (night) > 6% (day), 11% (night) > 6% (day), and 13% (night) > 12% (day)).

#### UHI variations by LCZ

Table 2 lists the average daytime and nighttime UHI values corresponding to other LCZ types, except water bodies (LCZF). As AST\_08 recorded the dynamic temperatures of the Earth's land surface, water bodies were not analyzed. LCZ5 and LCZA exhibited the lowest nighttime and daytime UHIs ( $-0.84$  and  $-5.31$ , respectively), whereas the highest nighttime and daytime UHIs were observed for LCZ7(2.20) and LCZ4(3.14), respectively. Figure 3 shows the differences in the daytime and nighttime UHI among the various LCZ types. The building types (LCZ1–LCZ10) generally exhibited higher UHI values, whereas the natural types (LCZA–LCZE) showed lower values. The average nighttime and daytime UHI values of the building types were  $1.11$  and  $2.77$  °C higher than those of the natural types, respectively. In addition, LCZ types with different vegetation coverage also exhibited differences in their daytime and nighttime UHIs. During the daytime, LCZ types with high vegetation coverage (LCZ10, A, B, and C) exhibited lower UHIs than LCZ types with low vegetation coverage (LCZ3, 4, and E). At night, the UHI values of LCZ7 and 8 were higher than those of LCZ1 and 2, which had lower levels of vegetation coverage. This is because the impervious surface of the city differs from the surfaces with vegetation, the reflectivity of solar radiation is small, the heat capacity is large, and the near-surface layer is relatively stable at night, resulting in poor heat dissipation, high stored heat, and a significant heat island effect.

#### Influence of sea and land breeze on UHI

Taking the offshore G3643 station as an example, typical (no significant changes in wind speed and direction) and atypical (diurnal changes in wind speed and direction) sea–land breeze days were analyzed, as shown in Fig. 4 (the typical sea–land breeze day was November 1, 2019, and the atypical sea–land breeze day was November 5, 2019). The results showed that the wind speed and direction were evidently disturbed by the onset of the sea breeze. The wind direction changed from offshore at the last moment to onshore, with an increase of  $>90^\circ$ , and the wind speed increased rapidly. However, as the sea breeze developed, the wind direction stabilized. In the onshore wind direction, the wind speed reached its daytime maximum at  $\sim 14:00$  (Beijing: GMT + 8). When the sea breeze ended, the wind direction

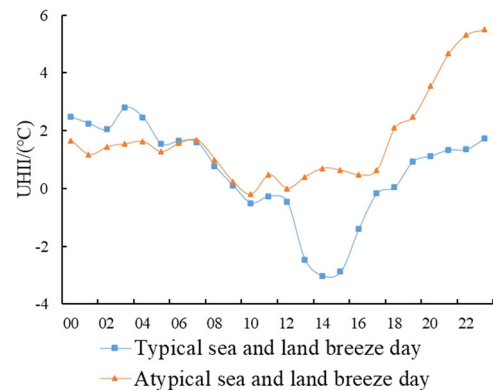


**Fig. 5** Daily variation characteristics of heat island intensity between typical sea–land breeze day and atypical sea–land breeze day. 00–22 in the horizontal axis represents time (hours).

suddenly shifted offshore, and the land breeze started developing. The wind speed reached its intraday maximum at  $\sim 03:00$  at night (Beijing: GMT + 8). For atypical sea and land breeze days, the dominant wind direction was southeast, and the wind speed remained at  $1 \text{ m s}^{-1}$ .

To compare the influence of the presence or absence of sea–land breeze on the intensity of heat islands, the daily variation characteristics of the heat island intensity on typical and atypical sea–land breeze days were analyzed by taking the offshore station (G3643) as an example. As shown in Fig. 5, the diurnal variation characteristics in the heat island intensity corresponding to the sea–land breeze day exhibited a “V”-shaped distribution. When the sea breeze started, the UHI reduced sharply, reaching its intraday minimum at  $\sim 14:00$  (Beijing: GMT + 8). This was considerably lower than that of the atypical sea–land breeze day. The UHI value of the land breeze day subsequently began to increase, stabilized at  $21:00$  (Beijing: GMT + 8), and then continued to increase, reaching its intraday maximum at  $\sim 03:00$  (Beijing: GMT + 8). This was higher than the UHI value on the atypical sea–land breeze day, but not on the typical sea–land breeze day. The UHI increased at  $18:00$  (Beijing: GMT + 8), reached its maximum at  $23:00$  (Beijing: GMT + 8), and gradually decreased before stabilizing. It began to decrease at  $07:00$  (Beijing: GMT + 8) and then remained relatively stable and low until  $17:00$  (Beijing: GMT + 8); however, it was higher than that on the typical sea–land breeze day. This showed that the sea breeze could cool the city

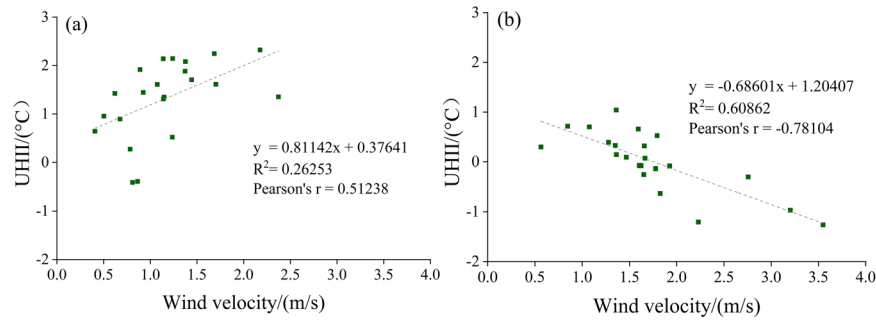


**Fig. 6** The relationship between sea–land breeze wind speed and heat island intensity. **a** Land breeze, **b** sea breeze.

**Table 3.** Summary of UHII in each LCZ in Shenzhen.

LCZ types	Daytime (°C)	Nighttime (°C)	LCZ types	Daytime (°C)	Nighttime (°C)
LCZ1	−0.03	1.31	LCZA	0.17	0.91
LCZ2	−0.04	1.33	LCZB	0.11	1.03
LCZ3	−0.04	1.30	LCZC	0.08	1.10
LCZ4	−0.01	1.33	LCZD	0.13	1.06
LCZ5	0.09	1.25	LCZE	0.04	1.17
LCZ6	−0.05	1.32	LCZF	0.12	0.99
LCZ7	0.09	1.40			
LCZ8	0.09	0.94			
LCZ9	−0.08	1.19			
LCZ10	0.11	1.07			

and alleviate the heat island effect, whereas the land breeze could moderately increase the strength of the heat island effect. Therefore, compared with the atypical sea–land breeze day, the daily UHI variations were greater on the typical sea–land breeze day.

Both sea and land breezes had a certain effect on UHI. To further analyze the mechanism between the sea–land breezes and UHI, we combined the UHIs during the start and end of the sea and land breezes to obtain the correlations between the average wind speed of the overall sea and land breezes and UHIs in Shenzhen (Fig. 6); subsequently, both passed the confidence test with a significance level of  $\alpha = 0.05$ . The sea breeze wind speed was negatively correlated with the UHI, with a correlation coefficient of  $-0.68601$ ; i.e., the greater the sea breeze wind speed, the smaller the UHI, indicating that the sea breeze alleviated the heat island effect. However, land breeze wind speed and UHI were positively correlated, with the correlation coefficient of  $0.81142$ ; i.e., the greater the wind speed, the greater the UHI. The  $R^2$  values between the sea and land wind speeds and UHI were  $0.60862$  and  $0.26253$ , respectively, indicating that the impact of sea breeze was stronger than that of a land breeze. As the sea breeze was accompanied by damp and cold air currents, the UHI effect was greatly reduced.

## DISCUSSION

Most of the currently used LCZ classification schemes employ the WUDAPT L0 method with a spatial resolution of  $100\text{ m}^{69}$  or remote sensing image data (spatial resolution of  $30\text{ m}–1\text{ km}$ ), combined with building data and other GIS analysis methods<sup>70,71</sup>. For example, Chen et al.<sup>70</sup> selected training samples based on MODIS and ASTER images, combined with Google Earth high-definition images. They then used the random forest method to perform LCZ classification to explore the spatial distribution of thermal environments in Guangzhou and Hong Kong, two of China's subtropical high-density cities; consequently, the two cities were

found to be clearly spatially resolved. Among these methods, the WUDAPT L0 approach appears to be more suitable for performing LCZ classification over large-scale areas; however, analyzing the internal differences in small- and medium-sized cities requires higher-precision data. Based on the GIS analysis, this study used land-use and urban building data, with a spatial resolution of  $10\text{ m}$ , to classify the LCZs. This approach resolved the low accuracy and yielded more comprehensive and accurate classification results. Additionally, this study referred to the LCZ classification scheme of Stewart & Oke<sup>40</sup> and combined the actual situation in Shenzhen to classify the buildings more finely, which can better reflect the effect of building height and density on the strength of the heat island.

The LCZ scheme was originally designed to use the difference in air temperature to quantify the intensity of the heat island<sup>39</sup>. However, the distribution of meteorological stations is uneven, and the acquired UHI cannot cover all LCZs. The UHI value of the study area ignores the differences within the city, and it is not convenient to study the effect of LCZs on UHI. This study also calculated the air temperature results (Table 3) and found that the UHI of the building type during the daytime was higher than that of the natural type. The difference between the building types was not obvious. Therefore, this article analyzed from the perspective of LST to reduce the influence of unknown interference factors that cause interference.

When analyzing the effect of sea and land breeze on UHI, this study used the air temperature values acquired from the meteorological stations. In addition, to illustrate the difference between air temperature and land surface temperature, the relationship of UHI with sea and land breezes was also calculated using land surface temperature (Fig. 7). The results (all passed the confidence test at the level of  $\alpha = 0.05$ ) showed that sea and the land breeze had a positive and negative correlation with UHI, respectively, but both the  $R^2$  values were small ( $3.44127\text{E}-6$  and  $0.03529$ , respectively), and the fitting effect was not ideal,

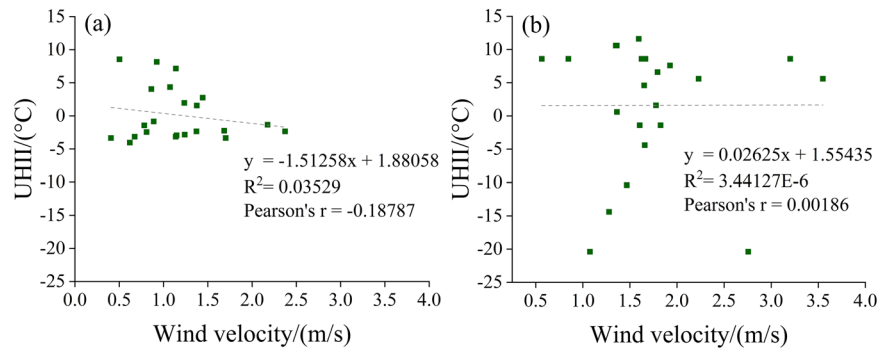


**Fig. 7** The relationship between sea-land breeze wind speed and heat island intensity. **a** Land breeze, **b** sea breeze.

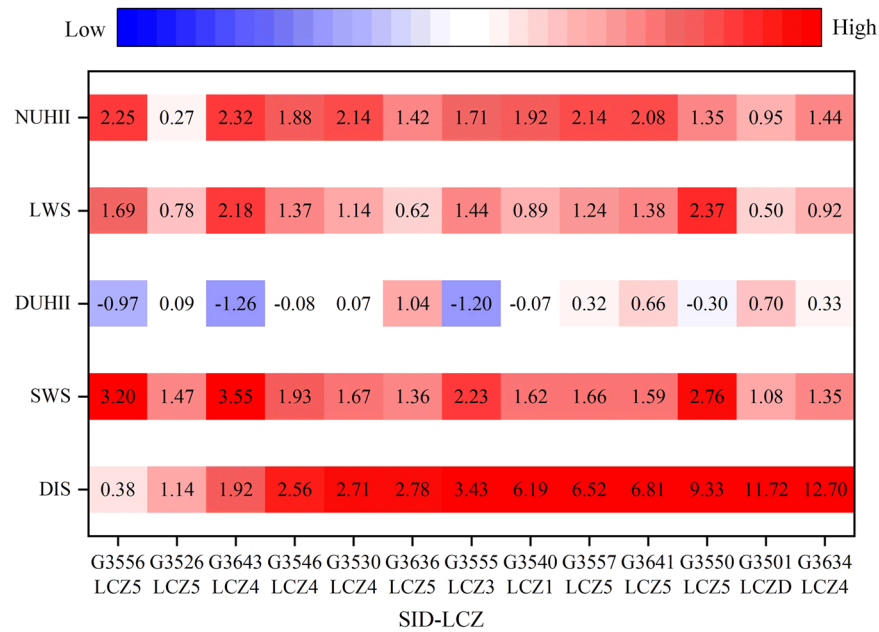


**Fig. 8** The relationship between day and night UHII and sea-land wind speed, LCZ types, and distance to coastline at various weather stations. SID-LCZ indicates the station number and the type of LCZ to which it belongs, DIS stands for the distance between the station and the coastline, SWS and LWS represent wind speed of sea and land, respectively, DUHII and NUHII, respectively, represent the intensity of day and night heat island.

indicating that the effect of sea and land breeze on UHII was not ideal from the perspective of LST (for Shenzhen).

Most previous studies have only focused on the effects of LCZs or sea-land breeze on UHIs<sup>72–74</sup>. Furthermore, the influencing mechanism of the UHII has rarely been investigated from the comprehensive perspective of the sea-land breeze and LCZ. Therefore, Zhou et al.<sup>75</sup> and Martinelli et al.<sup>76</sup> discussed the impacts of different LCZ types on the surface temperature from the perspective of LCZs by simultaneously qualitatively analyzing the impacts of sea and land breezes on urban temperatures in Sendai, Japan, and Bari, Italy, respectively. However, Sendai, Bari, and Shenzhen are characterized by different climate types, and differences in the LCZ distributions within these cities. In addition, they did not quantitatively analyze the effects of sea and land breezes on the UHII. Moreover, when analyzing the influences of sea and land breezes on UHII, they focused less on the differences between these two variables under different gradients. Therefore, based on the two directions of the sea and land breezes and LCZs, this study analyzed the impacts of different LCZ types on the UHII while also determining their correlation with UHII. The average daytime and nighttime UHII values of the building LCZ types were

1.11 and 2.77 °C higher than those of the natural types, respectively. Sea breezes alleviated the UHI effect, whereas land wind moderately enhanced the UHI effect. The linear regression coefficients between the sea and land breeze wind speeds and UHII were  $-0.68601$  and  $0.81142$ , respectively.

To further analyze the variations in the sea and land wind speeds under different gradients and the influences of different LCZ types on the UHI strength, ArcMap 10.4 (Environmental Systems Research Institute, California, USA) was used to calculate the distances of various meteorological stations from the coastline and analyze the effects of the sea and land wind speeds and LCZ types on the UHII (UHII is obtained by air temperature) from different gradient angles (Fig. 8). Regardless of the type of LCZ at the meteorological station, the overall trends in the sea breeze wind speed and UHII values were inversely proportional, i.e., the greater the sea breeze wind speed, the smaller the UHII. Moreover, for the same LCZ type, areas farther from the coastline had lower sea breeze wind speeds and greater UHII values. For example, stations G3643, G3546, G3530, and G3634 were all LCZ4 type, and their distances to the coastline were 1.9, 2.6, 2.7, and 12.7 km, respectively. The sea breeze wind speeds were G3643 ( $3.55 \text{ m s}^{-1}$ )

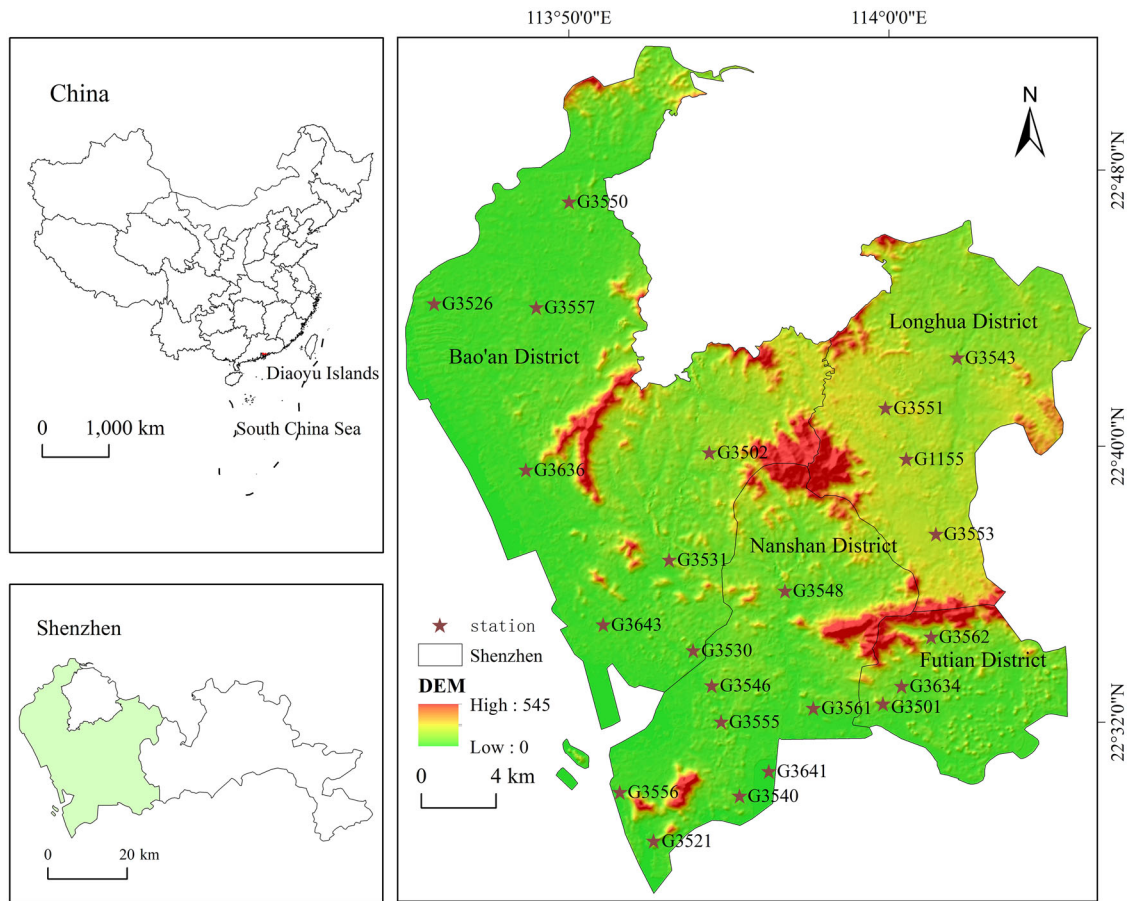


**Fig. 9** The location of study area (Shenzhen, China). All panels show the geographic location map of the study area. The upper left panel represents the distribution of the study area in China, the lower left panel represents of the study area the distribution in Shenzhen City, and the right panel shows the specific extent of the study area and the distribution of stations and DEM.

$> G3546 (1.93 \text{ m}\cdot\text{s}^{-1}) > G3530 (1.67 \text{ m}\cdot\text{s}^{-1}) > G3634 (1.35 \text{ m}\cdot\text{s}^{-1})$ , whereas the UHI values were  $G3643 (-1.26) < G3546 (-0.08) < G3530 (0.07) < G3634 (0.33)$ . In addition, the effect of the sea breeze on the UHI for different LCZ types was investigated. For example, stations G3550 and G3501 belonged to LCZ5 and LCZD, respectively. For the influences of different LCZ types on the UHI,  $\text{UHII}_{\text{LCZ5}} > \text{UHII}_{\text{LCZD}}$ ; however, the station results showed  $\text{UHII}_{\text{LCZ5}} < \text{UHII}_{\text{LCZD}}$ . This was primarily because the distance of G3550 from the coastline (9.3 km) was less than that of G3501 (11.7 km). Furthermore,  $V_{\text{LCZ5}}$  was more than  $V_{\text{LCZD}}$ , indicating that sea breezes can alleviate the UHI effect. However, the land breeze wind speed and UHI were relatively positively correlated, i.e., the land breeze wind speed increased as the UHI increased. Moreover, for the same type of LCZ, stations farther from the coastline had lower land breeze wind speeds and showed a lower decrease in the UHI. Similarly, considering stations G3643, G3546, G3530, and G3634 as examples, the land wind speed values were as follows:  $G3643 (2.18 \text{ m}\cdot\text{s}^{-1}) > G3546 (1.37 \text{ m}\cdot\text{s}^{-1}) > G3530 (1.14 \text{ m}\cdot\text{s}^{-1}) > G3634 (0.92 \text{ m}\cdot\text{s}^{-1})$ , whereas the UHI values were  $G3643 (2.32) > G3530 (2.14) > G3546 (1.88) > G3634 (1.44)$ . The two did not show a typical positive correlation, revealing that the positive correlation between the land breeze wind speed and UHI was not strong.

The urban spatial distribution of Shenzhen differs from that of Sendai (Japan), Tianjin, and other cities in China. Its urban center is near the coastline, and the suburbs are inland. Therefore, the conclusions drawn here may differ from those of other cities. The differences in the climate types may also cause differences in the

results. Thus, local conditions should be taken into consideration when performing LCZ divisions and calculating the correlations between sea and land breezes and the UHI.

This study primarily analyzed the effects of different LCZ types, typical and atypical sea–land breeze days, and different gradient sea–land wind speeds on daytime and nighttime UHI. Our results provide an important reference for urban planning and government decision-making. However, this study also has certain limitations. First, as the AST\_08 data do not contain water temperature information, the potential factors that can affect the strengths of UHIs were not taken into consideration. Second, due to time constraints associated with image acquisition, the daytime and nighttime UHIs recorded in this study were not obtained for the same days. Although they were acquired under clear weather conditions within the same month, various daily conditions may have caused partial differences in the results. Finally, this study only considered the impacts of the sea and land breezes on the daytime and nighttime UHIs only in November, and seasonal differences or the UHI mechanisms were not considered. Therefore, the seasonal and regional environmental differences in the sea and land breezes and daytime and nighttime UHIs should be further explored.

## METHODS

### Study area and data

Shenzhen (Fig. 9), also known as “Pengcheng,” is located in southern Guangdong, China, on the eastern bank of the Pearl River Estuary, with

**Table 4.** Data description.

Data types	Time	Resolution (m)	Sources	Pretreatment
Land-use data	2017	10	<a href="http://data.ess.tsinghua.edu.cn/">http://data.ess.tsinghua.edu.cn/</a>	-
Building data	2018	-	<a href="https://map.baidu.com/">https://map.baidu.com/</a>	Use the same Google Earth image to further correct and supplement the data.
AST_08	2018	90	<a href="https://search.earthdata.nasa.gov/">https://search.earthdata.nasa.gov/</a>	-
Weather station data	2019	-	<a href="https://opendata.sz.gov.cn/">https://opendata.sz.gov.cn/</a>	Calculate the basic information of automatic stations and calculate the monthly average sea and land wind speed at the station.
ASTER_GDEM	2009	30	<a href="http://www.gscloud.cn/">http://www.gscloud.cn/</a>	-
Administrative division data	2019	-	-	-

Daya Bay and Dapeng Bay to the east and the Pearl River Estuary and Lingding Ocean to the west. The terrain is high in the southeast and low in the northwest. Most of the area comprises low hills with gentle terraces. The region has a subtropical oceanic climate. Due to the strong influence of monsoons, the dominant wind direction is easterly-to-southeast, and southeasterly winds prevail in the summer. There are occasional monsoon lows and tropical cyclones. The northeast monsoon prevails during the remaining seasons. The weather is relatively dry, the climate is mild, and the annual average temperature is  $\sim 22.4^\circ\text{C}$ .

Data on land use, construction, administrative divisions, digital elevation models, Landsat remote sensing images, ASTER surface temperatures, and meteorological factors were used in this study (Table 4).

### LCZ classification

An LCZ refers to a combination of similar thermal environment characteristics based on urban surface properties and morphologies. However, the LCZ classification system and its standards are not static. This study used the results of previous studies<sup>39,40,50–52</sup>, along with the urban structure and architectural characteristics of Shenzhen, to establish its LCZ classification system. Thus, an LCZ system, comprising 16 categories, was constructed, which contained 10 buildings and six natural types (Table 5). Furthermore, the study area was divided into  $30 \times 30$  m grids using the fishing net tool in ArcGIS 10.4 (Environmental Systems Research Institute, California, USA). The building data were then mapped to the fishing net. Moreover, the building-type areas were divided according to two morphological indicators: building height and building density. The classification results were labeled under LCZ1–LCZ10. Among these, “dense” referred to a building density of  $>0.4$ , while “open” referred to a building density of  $<0.4$ . In addition, the natural type areas were divided using land-use data. The corresponding classification results were labeled as LCZA–LCZF.

### Sea and land wind speed

A sea–land breeze is a small-to-medium-scale thermal circulation caused by the temperature difference between the sea and land. It typically overlaps with the background wind field. Along the coastline of Shenzhen, the sea–land wind direction and monsoon wind direction overlap each other, which can easily lead to errors in assessing the sea–land winds. Therefore, effectively distinguishing the sea–land winds is crucial. This study referred to the sea and land wind distinction method proposed by Wei<sup>77</sup>. Thus, the wind was decomposed into a vector based on a trigonometric function, i.e.,  $u$  component in the east–west direction and  $v$  component in the north–south direction. The corresponding formulas are as follows:

$$u = V \cdot \sin D \quad (1)$$

$$v = V \cdot \cos D \quad (2)$$

where  $V$  is the measured wind speed at the weather station and  $D$  is the wind direction.

The winds were divided into the measured, system, and local winds. Among these, the measured wind comprised hourly data recorded by various meteorological stations, system wind comprised large-scale background wind recorded daily at each station, and local wind comprised mesoscale circulation, such as sea–land and valley wind. After the vector decomposition of the measured wind values, the 24 h average values of the  $u$  and  $v$  components were calculated. The daily average wind was obtained after synthesis, i.e., the system wind of a particular day. The measured and system wind values were calculated as the vector difference, i.e., the local wind. As this study did not consider the influence of valley wind, the calculated local wind comprised the sea and land wind. The specific formula is as follows:

$$\vec{V}_{dh} = \vec{V}_d + \vec{V}_h, \quad (3)$$





$$\vec{V}_d = \frac{1}{24} \sum_{h=0}^{23} \vec{V}_{dh}, \quad (4)$$

and

$$\vec{V}_h = \vec{V}_{dh} - \vec{V}_d. \quad (5)$$



**Table 5.** Definition and description of each LCZ type.

LCZ types	Descriptions	Examples	LCZ types	Descriptions	Examples
LCZ1	Compact super high-rise buildings (above 12 floors)		LCZA (Dense trees)	Dense coniferous forest and evergreen forest.	
LCZ2	Compact high-rise buildings (10-12 floors)		LCZB (Scattered trees)	Sparse coniferous forest and evergreen forest.	
LCZ3	Compact middle and high-rise buildings (7-9 floors)		LCZC (Shrub)	Open arrangement of bushes, shrubs, and short, woody trees.	
LCZ4	Compact mid-rise buildings (4-6 floors)		LCZD (Low plants)	Grassland or herbaceous plants/crops. Few or no trees.	
LCZ5	Compact low-rise buildings (1-3 floors)		LCZE (Bare soil or sand)	Featureless landscape of soil or sand cover. Few or no trees or plants.	
LCZ6	Open super high-rise buildings (above 12 floors)		LCZF (Water)	Large, open water bodies or small bodies.	
LCZ7	Open high-rise buildings (10-12 floors)				
LCZ8	Open middle and high-rise buildings (7-9 floors)				
LCZ9	Open mid-rise buildings (4-6 floors)				
LCZ10	Open low-rise buildings (1-3 floors)				

where  $\vec{V}_{dh}$  is the actually measured wind vector at a given time,  $h$ , on day  $d$ ,  $\vec{V}_d$  is the system wind vector on day  $d$ , and  $\vec{V}_h$  is the local wind vector at a given time,  $h$ , on day  $d$ .

Further, in this study, data of November 2019 acquired from the meteorological stations in the Futian, Bao'an, Longhua, and Nanshan districts were analyzed (except for the adjacent mountains). Based on statistics, 02:00–09:00 (Beijing: GMT + 8) was selected as the duration for land winds, while 14:00–21:00 (Beijing: GMT + 8) time was selected as the duration for sea winds; subsequently, the average wind speeds for the sea and land winds during these times were calculated.

**UHII**

In addition to the LCZ theory, the definition of the heat island effect changed. When Stewart and Oke<sup>40</sup> proposed the LCZ theory, they also redefined the intensity of the heat island effect. This study adopted the redefinition of the intensity of the heat island effect proposed by Stewart and Oke<sup>40</sup>. The formula is as follows:

$$UHII_{LCZX} = T_{LCZX} - T_{LCZD}, \tag{6}$$

where  $UHII_{LCZX}$  represents the heat island effect intensity of LCZX and  $T_{LCZX}$  and  $T_{LCZD}$  are the surface temperature of the type X and D LCZs,

respectively. In other words, the intensity of the heat island effect is the temperature difference between each LCZ and the LCZD type (low vegetation).

## DATA AVAILABILITY

The datasets aggregated and/or analyzed during the current study are available from the corresponding author on reasonable request. Land-use dataset are available at <http://data.ess.tsinghua.edu.cn/><sup>78</sup>. Building data are available at <https://map.baidu.com/>. AST\_08 dataset are available at <https://search.earthdata.nasa.gov/>. Weather station data are available at <https://opendata.sz.gov.cn/>. ASTER\_GDEM data are available at <http://www.gscloud.cn/>.

Received: 10 August 2021; Revised: 27 February 2022; Accepted: 8 April 2022;

Published online: 30 May 2022

## REFERENCES

- Mahtta, R. et al. Urban land expansion: the role of population and economic growth for 300+ cities. *npj Urban Sustain.* **2**, 1–11 (2022).
- Joose, S., Hensle, L., Boonstra, W. J., Ponzelar, C. & Olsson, J. Fishing in the city for food—a paradigmatic case of sustainability in urban blue space. *npj Urban Sustain.* **1**, 1–8 (2021).
- Strokal, M. et al. Urbanization: an increasing source of multiple pollutants to rivers in the 21st century. *npj Urban Sustain.* **1**, 24 (2021).
- Jiang, H. et al. An assessment of urbanization sustainability in China between 1990 and 2015 using land use efficiency indicators. *npj Urban Sustain.* **1**, 34 (2021).
- Yang, J., Hu, L. & Wang, C. Population dynamics modify urban residents' exposure to extreme temperatures across the United States. *Sci. Adv.* **5**, eaay3452 (2019).
- Hoag, H. How cities can beat the heat. *Nature* **524**, 402–404 (2015).
- Zhao, L. et al. Interactions between urban heat islands and heat waves. *Environ. Res. Lett.* **3**, 034003 (2018).
- Tan, J. et al. The urban heat island and its impact on heat waves and human health in Shanghai. *Int. J. Biometeorol.* **54**, 75–84 (2010).
- Dagilis, A. J. & Matute, D. R. Incompatibilities between emerging species. *Science* **368**, 710–711 (2020).
- Hulley, G. C., Dousset, B. & Kahn, B. H. Rising trends in heatwave metrics across Southern California. *Earth's Future* **8**, e1480E–e2020E (2020).
- Lange, S. et al. Projecting exposure to extreme climate impact events across six event categories and three spatial scales. *Earth's Future* **8**, e1616E–e2020E (2020).
- Sagris, V. & Sepp, M. Landsat-8 TIRS data for assessing urban heat island effect and its impact on human health. *IEEE Geosci. Remote Sens. Lett.* **14**, 2385–2389 (2017).
- Yang, J. et al. Projecting heat-related excess mortality under climate change scenarios in China. *Nat. Commun.* **12**, 1–11 (2021).
- Howard, L. *The Climate of London*. (Harvey and Dorton, 1833).
- Weng, Q. Thermal infrared remote sensing for urban climate and environmental studies: Methods, applications, and trends. *ISPRS J. Photogramm. Remote Sens.* **64**, 335–344 (2009).
- Liu, X. et al. Spatiotemporal patterns of summer urban heat island in Beijing, China using an improved land surface temperature. *J. Cleaner Product.* **257**, 120529 (2020).
- Luan, X. et al. Remote sensing and social sensing data reveal scale-dependent and system-specific strengths of urban heat island determinants. *Remote Sens. (Basel, Switzerland)* **12**, 391 (2020).
- Pathak, C. et al. The effects of land indices on thermal state in surface urban heat island formation: a case study on Agra City in India using remote sensing data (1992–2019). *Earth Syst. Environ.* **5**, 135–154 (2021).
- Tepanosyan, G. et al. Studying spatial-temporal changes and relationship of land cover and surface Urban Heat Island derived through remote sensing in Yerevan, Armenia. *Build. Environ.* **187**, 107390 (2021).
- Yuan, C. et al. Mitigating intensity of urban heat island by better understanding on urban morphology and anthropogenic heat dispersion. *Building Environ.* **176**, 106876 (2020).
- Yue, W., Liu, X., Zhou, Y. & Liu, Y. Impacts of urban configuration on urban heat island: an empirical study in China mega-cities. *Sci. Total Environ.* **671**, 1036–1046 (2019).
- Yue, W., Qiu, S., Xu, H., Xu, L. & Zhang, L. Polycentric urban development and urban thermal environment: a case of Hangzhou, China. *Landsc. Urban Plan.* **189**, 58–70 (2019).
- Elmes, A. et al. Mapping spatiotemporal variability of the urban heat island across an urban gradient in Worcester, Massachusetts using in-situ Thermochrons and Landsat-8 Thermal Infrared Sensor (TIRS) data. *GISci. Remote Sens.* **57**, 845–864 (2020).
- Firozjahi, M. K., Fatholouloumi, S., Kiavarz, M., Arsanjani, J. J. & Alavipanah, S. K. Modelling surface heat island intensity according to differences of biophysical characteristics: a case study of Amol city, Iran. *Ecol. Indicators* **109**, 105816 (2020).
- Guo, A. et al. Influences of urban spatial form on urban heat island effects at the community level in China. *Sustain. Cities Soc.* **53**, 101972 (2020).
- Luan, X. et al. Remote sensing and social sensing data reveal scale-dependent and system-specific strengths of urban heat island determinants. *Remote Sens.* **12**, 391 (2020).
- Monteiro, F. F., Gonçalves, W. A., Andrade, L. D. M. B., Villavicencio, L. M. M. & Dos Santos Silva, C. M. Assessment of Urban Heat Islands in Brazil based on MODIS remote sensing data. *Urban Clim.* **35**, 100726 (2021).
- Peres, L. D. F., Lucena, A. J. D., Rotunno Filho, O. C. & França, J. R. D. A. The urban heat island in Rio de Janeiro, Brazil, in the last 30 years using remote sensing data. *Int. J. Appl. Earth Observ. Geoinform.* **64**, 104–116 (2018).
- Qiao, Z. et al. The impact of urban renewal on land surface temperature changes: a case study in the Main City of Guangzhou, China. *Remote Sens.* **12**, 794 (2020).
- Sekertekin, A. & Bonafoni, S. Land surface temperature retrieval from landsat 5, 7, and 8 over rural areas: assessment of different retrieval algorithms and emissivity models and toolbox implementation. *Remote Sens.* **12**, 294 (2020).
- Yang, J. et al. Evaluation of seven atmospheric profiles from reanalysis and satellite-derived products: implication for single-channel land surface temperature retrieval. *Remote Sens. (Basel, Switzerland)* **12**, 791 (2020).
- Su, M. A., Ngarambe, J., Santamouris, M. & Yun, G. Y. Empirical evidence on the impact of urban overheating on building cooling and heating energy consumption. *iScience* **24**, 102495 (2021).
- Jing, R., Hastings, A. & Guo, M. Sustainable design of urban rooftop food-energy-land nexus. *iScience* **23**, 101743–101743 (2020).
- Zhou, B., Rybski, D. & Kropp, J. P. The role of city size and urban form in the surface urban heat island. *Sci. Rep.* **7**, 1–9 (2017).
- Zhang, R. Cooling effect and control factors of common shrubs on the urban heat island effect in a southern city in China. *Sci. Rep.* **10**, 1–8 (2020).
- Li, D. et al. Urban heat island: aerodynamics or imperviousness? *Sci. Adv.* **5**, eaau4299 (2019).
- Han, Q., Keeffe, G., Caplat, P. & Simson, A. Cities as hot stepping stones for tree migration. *npj Urban Sustain.* **1**, 12 (2021).
- Ren, J. et al. Exploring thermal comfort of urban buildings based on local climate zones. *J. Clean. Product.* **340**, 130744 (2022).
- Stewart, I. D., Oke, T. R. & Krayenhoff, E. S. Evaluation of the 'local climate zone' scheme using temperature observations and model simulations. *Int. J. Climatol.* **34**, 1062–1080 (2014).
- Stewart, I. D. & Oke, T. R. Local climate zones for urban temperature studies. *Bull. Am. Meteorol. Soc.* **93**, 1879–1900 (2012).
- Giridharan, R. & Emmanuel, R. The impact of urban compactness, comfort strategies and energy consumption on tropical urban heat island intensity: a review. *Sustain. Cities Soc.* **40**, 677–687 (2018).
- Kaloustian, N. & Bechtel, B. Local climatic zoning and urban heat island in Beirut. *Proc. Eng.* **169**, 216–223 (2016).
- Kotharkar, R. & Bagade, A. Local climate zone classification for Indian cities: A case study of Nagpur. *Urban Clim.* **24**, 369–392 (2018).
- Anjos, M., Targino, A. C., Krecl, P., Oukawa, G. Y. & Braga, R. F. Analysis of the urban heat island under different synoptic patterns using local climate zones. *Building Environ.* **185**, 107268 (2020).
- Berlessova, A. A. & Konstantinov, P. I. Local climate zones in the city of Nur-Sultan (Kazakhstan) and their connections with urban heat island and thermal comfort. *IOP Publishing.* **611**, 12060 (2020).
- Chieppa, J., Bush, A. & Mitra, C. Using "Local Climate Zones" to detect urban heat island on two small cities in Alabama. *Earth Interact.* **22**, 1–22 (2018).
- Jin, L. et al. Block-based local climate zone approach to urban climate maps using the UDC model. *Build. Environ.* **186**, 107334 (2020).
- Kotharkar, R., Bagade, A. & Singh, P. R. A systematic approach for urban heat island mitigation strategies in critical local climate zones of an Indian city. *Urban Clim.* **34**, 100701 (2020).
- Yang, X. et al. Impact of urban heat island on energy demand in buildings: local climate zones in Nanjing. *Appl. Energy* **260**, 114279 (2020).
- Bechtel, B. et al. Mapping local climate zones for a worldwide database of the form and function of cities. *ISPRS Int. J. Geo Inform.* **4**, 199–219 (2015).
- Bechtel, B. et al. SUHI analysis using Local Climate Zones—a comparison of 50 cities. *Urban Clim.* **28**, 100451 (2019).
- Beck, C. et al. Air temperature characteristics of local climate zones in the Augsburg urban area (Bavaria, southern Germany) under varying synoptic conditions. *Urban Clim.* **25**, 152–166 (2018).
- Ochola, E. M. et al. Inter-local climate zone differentiation of land surface temperatures for Management of Urban Heat in Nairobi City, Kenya. *Urban Clim.* **31**, 100540 (2020).

54. Oliveira, A., Lopes, A. & Niza, S. Local climate zones in five southern European cities: An improved GIS-based classification method based on Copernicus data. *Urban Clim.* **33**, 100631 (2020).
55. Yang, J. et al. Investigating the diversity of land surface temperature characteristics in different scale cities based on local climate zones. *Urban Clim.* **34**, 100700 (2020).
56. Zhao, C. Linking the local climate zones and land surface temperature to investigate the surface urban heat island, a case study of San Antonio, Texas, US. *ISPRS Ann. Photogramm. Remote Sens. Spatial Inform. Sci.* **3**, 277–283 (2018).
57. Zhao, C., Jensen, J. L. R., Weng, Q., Currit, N. & Weaver, R. Use of Local Climate Zones to investigate surface urban heat islands in Texas. *GISci. Remote Sens.* **57**, 1083–1101 (2020).
58. He, B., Wang, J., Liu, H. & Ulpiani, G. Localized synergies between heat waves and urban heat islands: Implications on human thermal comfort and urban heat management. *Environ. Res.* **193**, 110584 (2021).
59. Luo, X., Yang, J., Sun, W. & He, B. Suitability of human settlements in mountainous areas from the perspective of ventilation: a case study of the main urban area of Chongqing. *J. Clean. Prod.* **310**, 127467 (2021).
60. Ren, C. et al. Investigating the urban heat and cool island effects during extreme heat events in high-density cities: A case study of Hong Kong from 2000 to 2018. *Int. J. Climatol.* **41**, 6736–6754 (2021).
61. Xie, P., Yang, J., Sun, W., Xiao, X. & Cecilia Xia, J. Urban scale ventilation analysis based on neighborhood normalized current model. *Sustain. Cities Soc.* **80**, 103746 (2022).
62. He, B., Ding, L. & Prasad, D. Outdoor thermal environment of an open space under sea breeze: A mobile experience in a coastal city of Sydney, Australia. *Urban Clim.* **31**, 100567 (2020).
63. Park, M. & Chae, J. Features of sea-land-breeze circulation over the Seoul Metropolitan Area. *Geosci. Lett.* **5**, 1–12 (2018).
64. Wang, Y. et al. Impact of land surface heterogeneity on urban heat island circulation and sea-land breeze circulation in Hong Kong. *J. Geophys. Res. Atmos.* **8**, 4332–4352 (2017).
65. Zhou, Y. et al. Sea breeze cooling capacity and its influencing factors in a coastal city. *Building Environ.* **166**, 106408 (2019).
66. Ramamurthy, P. & Sangobanwo, M. Inter-annual variability in urban heat island intensity over 10 major cities in the United States. *Sustain. Cities Soc.* **26**, 65–75 (2016).
67. Wang, Q., Zhang, C., Ren, C., Hang, J. & Li, Y. Urban heat island circulations over the Beijing-Tianjin region under calm and fair conditions. *Build. Environ.* **180**, 107063 (2020).
68. Shen, L., Sun, J. & Yuan, R. Idealized large-eddy simulation study of interaction between urban heat island and sea breeze circulations. *Atmos. Res.* **214**, 338–347 (2018).
69. Dian, C., Pongrácz, R., Dezső, Z. & Bartholy, J. Annual and monthly analysis of surface urban heat island intensity with respect to the local climate zones in Budapest. *Urban Clim.* **31**, 100573 (2020).
70. Chen, X., Xu, Y., Yang, J., Wu, Z. & Zhu, H. Remote sensing of urban thermal environments within local climate zones: a case study of two high-density subtropical Chinese cities. *Urban Clim.* **31**, 100568 (2020).
71. Yang, J. et al. Understanding land surface temperature impact factors based on local climate zones. *Sustain. Cities Soc.* **69**, 102818 (2021).
72. Mughal, M. O., Li, X. & Norford, L. K. Urban heat island mitigation in Singapore: evaluation using WRF/multilayer urban canopy model and local climate zones. *Urban Clim.* **34**, 100714 (2020).
73. Skarbit, N., Stewart, I. D., Unger, J. & Gál, T. Employing an urban meteorological network to monitor air temperature conditions in the 'local climate zones' of Szeged, Hungary. *Int. J. Climatol.* **37**, 582–596 (2017).
74. Zhang, Y., Zhang, J., Zhang, X., Zhou, D. & Gu, Z. Analyzing the characteristics of UHI (Urban Heat Island) in summer daytime based on observations on 50 sites in 11 LCZ (Local Climate Zone) Types in Xi'an, China. *Sustainability* **13**, 83 (2021).
75. Zhou, X. et al. Evaluation of urban heat islands using local climate zones and the influence of sea-land breeze. *Sustain. Cities Soc.* **55**, 102060 (2020).
76. Martinelli, A., Kolokotsa, D. & Fiorito, F. Urban heat island in Mediterranean coastal cities: the case of Bari (Italy). *Climate* **8**, 79 (2020).
77. Wei, C. Analysis on the characteristics of sea and land breeze climate in coastal areas of Jiangsu coastal areas. (Nanjing University of Information Technology, 2012).
78. Gong, P. et al. Stable classification with limited sample: transferring a 30-m resolution sample set collected in 2015 to mapping 10-m resolution global land cover in 2017. *Sci. Bull.* **64**, 370–373 (2019).

## ACKNOWLEDGEMENTS

This research study was supported by the National Natural Science Foundation of China (grant no. 41771178, 42030409), the Fundamental Research Funds for the Central Universities (grant nos. N2111003), Basic Scientific Research Project (Key Project) of the Education Department of Liaoning Province (grant no. LJKZ0964), the Second Tibetan Plateau Scientific Expedition and Research Program (STEP) (grant no. 2019QZKK1004), and Innovative Talents Support Program of Liaoning Province (Grant No. LR2017017).

## AUTHOR CONTRIBUTIONS

J.Y. contributed to all aspects of this work; J.X. wrote the main manuscript text, Y.Z., X. X., and J.C.X. conducted the experiment and analyzed the data.

## COMPETING INTERESTS

The authors declare no competing interests

## ADDITIONAL INFORMATION

**Correspondence** and requests for materials should be addressed to Jun Yang or Yuqing Zhang.

**Reprints and permission information** is available at <http://www.nature.com/reprints>

**Publisher's note** Springer Nature remains neutral with regard to jurisdictional claims in published maps and institutional affiliations.



**Open Access** This article is licensed under a Creative Commons Attribution 4.0 International License, which permits use, sharing, adaptation, distribution and reproduction in any medium or format, as long as you give appropriate credit to the original author(s) and the source, provide a link to the Creative Commons license, and indicate if changes were made. The images or other third party material in this article are included in the article's Creative Commons license, unless indicated otherwise in a credit line to the material. If material is not included in the article's Creative Commons license and your intended use is not permitted by statutory regulation or exceeds the permitted use, you will need to obtain permission directly from the copyright holder. To view a copy of this license, visit <http://creativecommons.org/licenses/by/4.0/>.

© The Author(s) 2022